

# Damage Nucleation in Nuclear Graphite under Biaxial Flexural Loading

M. Mostafavi<sup>1</sup>, J. Duff<sup>1</sup>, R. Delorme<sup>1,2</sup>, T.J. Marrow<sup>1</sup>

<sup>1</sup>Materials Performance Centre, The University of Manchester, Manchester, UK,  
[M.Mostafavi@manchester.ac.uk](mailto:M.Mostafavi@manchester.ac.uk), [Jonthan.Duff@manchester.ac.uk](mailto:Jonthan.Duff@manchester.ac.uk),  
[James.Marrow@manchester.ac.uk](mailto:James.Marrow@manchester.ac.uk)

<sup>2</sup>Graduate Engineering School in Materials, Caen (ENSICAEN), France,  
[rdelorme@ecole.ensicaen.fr](mailto:rdelorme@ecole.ensicaen.fr)

**ABSTRACT** *Test specimens of graphite are known to exhibit sensitivity to stress state, such as a difference between their flexural and tensile strengths under uniaxial loading. Biaxial flexural loading is representative of the stress state in some regions of graphite components in nuclear fission reactors, where loading develops from fast neutron irradiation-induced dimensional change and thermal strains. Study of the behaviour of the inherent defects that determine strength variability requires in-situ detection of crack nucleation and propagation. To this end, digital image correlation (DIC) was used to monitor the evolution of strain fields and the nucleation and propagation of cracks on the surface of large samples of nuclear graphite. DIC is a full-field optical technique, used to measure surface displacements with high resolution and precision. An equi-biaxial ring-on-ring flexural test setup has been developed for large disc specimens of nuclear graphite along with the conventional four-point-bend test. The observed 17% reduction in mean flexural strength for equi-biaxial loading, relative to uniaxial loading, may be explained by a critical strain energy release rate for fracture.*

## INTRODUCTION

Graphite is used in several designs of nuclear fission reactors (e.g. the Advanced Gas reactors in the UK, the Pebble Bed Modular Reactor and proposed high temperature Generation IV designs) as a neutron moderator and reflector. Its structural integrity is important for safe operation, as irradiation-induced dimensional strains and thermal strains cause tensile stress, and irradiation damage can be detrimental to strength. Crack nucleation may therefore occur with prolonged operation.

One element required for evaluation of the graphite fracture behaviour under realistic loading conditions is an understanding of the effect of stress state on strength. Test specimens of quasi-brittle materials, such as nuclear graphite, are well known to exhibit sensitivity to stress state. Biaxial loading is also more representative of the loading in some regions of graphite components.

A wide range of models have been proposed for the fracture of graphite, from simple [1] to the more complex [2]. However, there is still ambiguity in the fracture process of graphite. The widely accepted deterministic theory for fracture of graphite defines a

critical maximum principal stress (or strain). However, due to the heterogeneity of graphite, the local maximum principle strain distribution can be noticeably different in similar specimens under identical loading condition. Therefore, knowledge of both the size and spatial distributions of significant flaws in the microstructure is important. This can be achieved through in-situ observation of the full-field displacements on the surface of samples, such as via electronic speckle pattern interferometry [3] and digital image correlation (DIC) [4]. DIC is based on recognizing and comparing specific features in both deformed and undeformed bodies to calculate their displacement. By differentiating the displacement field, the strain field can be obtained.

Several methods can be used to induce a biaxial stress field. A cruciform specimen under two perpendicular loadings is a common method. A disadvantage is that crack initiation may not take place on the surface, which is essential for DIC analysis. In addition, controlling two sets of actuators to apply equi-biaxial loading in displacement control is difficult. A more simple method is to use the flexural ring-on-ring loading configuration [5]. This has been developed in the present study, for observation of crack nucleation and propagation by DIC. Comparison is made between the fracture behaviour of graphite in biaxial flexural loading condition with the uniaxial flexural (four-point-bend) loading. A finite element analysis was conducted first to compare the fracture parameters of a semi-elliptical crack under uniaxial and equi-biaxial loadings.

## FINITE ELEMENT STUDY

The assumption is that damage propagates from defects that can be approximated as semi-elliptical shallow cracks [4]. Models containing such cracks, under uniaxial four-point-bend and biaxial flexure, were created using Abaqus/standard V. 6.9 [6]. Figure 1 illustrates a typical semi-elliptical crack. Figure 2a and Figure 2b show the FE mesh of uniaxial and biaxial models respectively ( $2c=10\text{mm}$  and  $a=2\text{mm}$ ).

Table 1- Dimensions of the models (thickness  $t$ , 10 mm, support radius 4 mm)

Rectangular specimen				Disc specimen		
Width ( $2W$ )	Height ( $2h$ )	Inner support span ( $2S_i$ )	Outer support span ( $2S_o$ )	Diameter ( $2R$ )	Inner support radius ( $2R_i$ )	Outer support radius ( $2R_o$ )
150mm	150mm	60mm	140mm	350mm	150mm	300mm

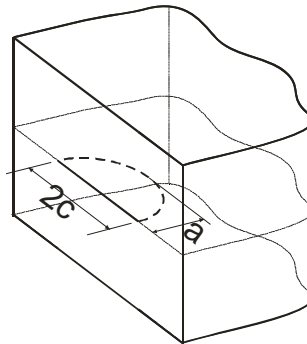


Figure 1- schematic view of a semi-elliptical crack

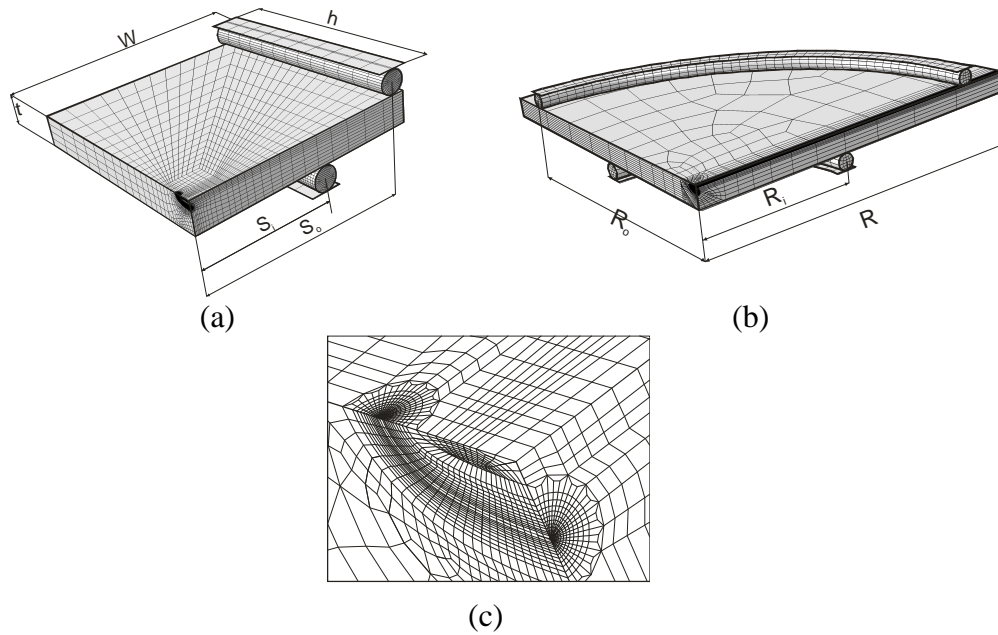


Figure 2- Finite element model of semi-elliptical crack under (a) four point bend (b) ring-on-ring (c) crack tip details

Using symmetry, one quarter of each sample was modelled with appropriate boundary conditions. The graphite was defined as a linear elastic material with typical mechanical properties  $E=10900$  MPa and  $\nu=0.21$  [7]. The supports are hyperelastic rubber, defined by the Mooney-Rivlin equation with values  $C_{10}=3.2$ ,  $C_{01}=0.8$  and  $D_1=1$ . A concentrated mesh with collapsed elements was used at the crack tip (Figure 2c). The loading was modelled by applying a displacement on a rigid body that was in contact with the rubber supports, which were in contact with the graphite sample. A total number of 14649 quadratic brick elements were used to simulate the disc specimen and 29210 similar elements were employed for the rectangular specimen.

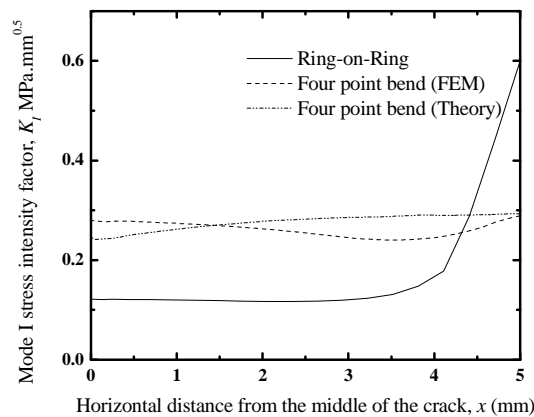


Figure 3- Mode I Stress intensity factor along the crack front for a semi-elliptical crack under uniaxial and equi-biaxial flexural loading (same surface stress and moment)

To verify the model, the predicted stress distribution on the surface of non-cracked samples was compared with analytical solutions [8] with agreement within 2%. Loading conditions were selected to apply an equal flexural stress at the surface of both models. The dimensions of the specimens are reported in Table 1. The mode I stress intensity factor along the crack front was calculated using Abaqus through the contour integral method [9], and is shown in Figure 3. The FE model was compared with the Newman and Raju [10] numerical solution for the same crack geometry under uniaxial bending. The stress intensity factor is highest at the surface for each case. For uniaxial loading, there is agreement (within 15%) between the FE and numerical solution. Differences between the FE and numerical solution in four point bending may be due to approximations in the numerical solution [10]. For biaxial loading the stress intensity factor on the surface is much higher, and is significantly lower elsewhere. This suggests a greater tendency for crack propagation along the surface, which may be monitored readily by the DIC technique.

## **EXPERIMENTS**

Experiments were carried out to calibrate the effects of relative vertical displacements on DIC displacement measurement, and then to perform four point bend uniaxial and ring-on-ring equi-biaxial fracture tests. The test setup is shown in Figure 4. A 4 MPixel 14 bit camera with a 50 mm objective lens was used to monitor the area of constant bending moment on each sample (approximately 100 mm × 100 mm)

### ***Calibration Tests***

The calibration tests were conducted using PMMA (i.e. Perspex). PMMA samples without cracks were loaded in uniaxial and equi-biaxial geometries with the same dimensions as the graphite test specimens. In flexural testing, the samples deflect noticeably in the centre, relative to supports. Parallax effects due to non-uniform displacement towards the camera cause an artificial strain field in the DIC analysis. This was calibrated by moving an unloaded disc toward the camera to calculate the apparent strain. Figure 5 shows the resulting strain in one direction ( $\epsilon_{xx}$ ), calculated by DIC for a window size of 128×128 pixels, with 0% overlap. No meaningful variation was observed with strain in the y direction. The effect of a tilted surface was also found to be negligible in comparison to other strains.

### ***Uniaxial Fracture Testing***

Fourteen four-point-bend uniaxial graphite samples were tested at displacement rate of 0.2 mm/min. Each specimen measured ( $2W \times 2h \times t$ ) 200 mm × 100 mm × 10 mm, with inner and outer spans of 90 mm and 180 mm. The support rollers were stainless steel in four point bend tests. FE analysis showed a less than 7% difference in the strain field at the points of contact caused by changing the rubber supports to steel, with negligible effects elsewhere. They were therefore used for convenience. Images were recorded at 1 Hz (typically 500 images per test). Focus was maintained at a position approximately 30mm from the sample centre. The flexural strength ( $\sigma_f$ ) was calculated using Eq. 1.

$$\sigma_f = \frac{3F_f (S_o - S_i)}{ht^2} \quad (1)$$

### ***Biaxial Fracture Testing***

Nine disc shaped graphite samples were tested using the ring-on-ring configuration. The diameter (2R) of the samples was 350 mm. The diameters of the inner (2b) and outer (2a) support rings were 150 mm and 300 mm. Viton rubber O-rings were used as supports to minimize the contact stresses, which was particularly important for these large specimens. The displacement and imaging conditions were as before, with typically 2000 images per test. The flexural strength was calculated using Eq. (2).[8]:

$$\sigma_f = \frac{3(1+\nu)}{2\pi t^2} F_f \left[ \ln\left(\frac{R_o}{R_i}\right) + \frac{(1-\nu)(R_o^2 - R_i^2)}{(1+\nu)2R^2} \right] \quad (2)$$

Following testing, Eq. (3) was employed to calculate the probability of fracture as a function of flexural strength (Figure 6). An average mean strength reduction of 17% was observed between the uniaxial and equi-biaxial conditions.

$$P_f = \frac{i-0.5}{N} \quad (3)$$

where  $P_f$  is the fracture probability,  $N$  is the total number of tested samples and  $i$  is the sample number, ranked in strength.

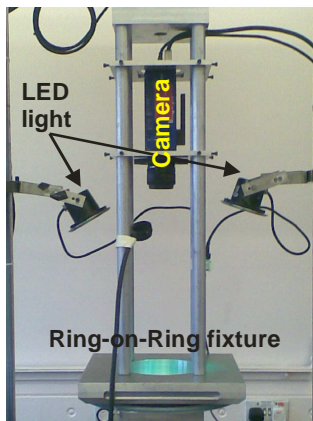


Figure 4- Test setup

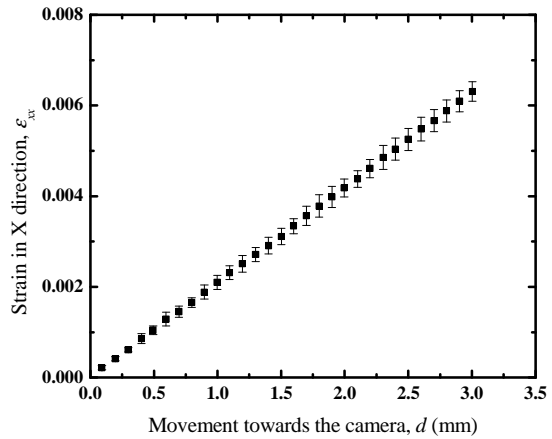


Figure 5- Evaluation of the strain along x axis vs. the movement toward the camera

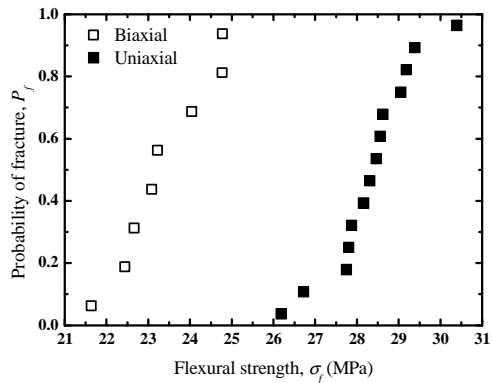


Figure 6- Fracture probability of graphite in uniaxial axial and biaxial loadings.

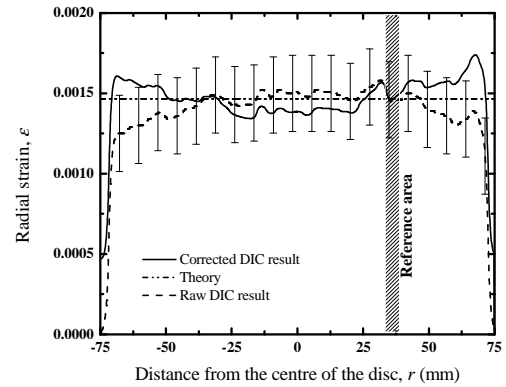


Figure 7- Radial strain distribution of a disc specimen under biaxial loading at  $F=1240N$

## DIC ANALYSIS

DIC was used to evaluate the evolution of surface displacements, and to detect crack nucleation and propagation by analysis of the strain field [4]. The LA Vision Davis software was used (Version 7.2). Multiple interrogation analysis with a window size of  $256 \times 256$  pixels at an overlap of 0% with 2 passes, followed by  $64 \times 64$  pixel windows at an overlap of 25% with 4 passes was found to give the best results in terms of image resolution and displacement accuracy.

The measured surface strain field for a PMMA sample under equi-biaxial flexure was compared to the analytical solution [8] to verify the test procedure and also the DIC analysis. Typical properties of PMMA ( $E=3100$  MPA,  $\nu=0.35$ ) were assumed. For example, the radial strain ( $\epsilon_{rr}$ ), between the inner and outer supports is calculated to be 0.1465% [8] at a load  $F=1240N$ , which was the maximum load applied. Figure 7 shows a good correlation between the predicted (i.e. theory) and measured (i.e. DIC) strain, although there are discrepancies, particularly towards the edge of the observed region where the measured strain is lower than predicted.

At the maximum load, the centre of the PMMA sample was calculated [8] to be 0.3 mm closer to the camera than the support positions. The calibration experiments (Figure 5) recorded an apparent strain of 0.002105 per mm of relative displacement, which was used to correct the raw DIC data. The focus position (30 mm from the centre) was taken as reference for the correction. The corrected strain is shown in Figure 7, which shows the effect of curvature is small compared to the experimental noise. This noise (0.024%) was evaluated from the RMS error in strain obtained by DIC analysis of successive images recorded of a sample with no load change. DIC analysis was applied to all images using the same parameters as the calibration experiments. Examples of the maximum principal strain fields are seen in Figure 8. The banding is an artefact of DIC at low strains. The locations of the inner supports are marked. Cracks could be detected shortly prior to failure on the surface of both uniaxial and equi-biaxial samples as regions of high strain (typically 1% and 1.5% respectively).

## DISCUSSION

DIC analysis allows the evolution of crack length and opening displacement to be studied. A preliminary analysis is presented here. Figure 9a shows data for the longest detected crack in three examples of each geometry. It shows that cracks nucleate and propagate along the surface, but there is no relationship between surface crack length and flexural strength. Figure 9b, on the other hand, shows the maximum crack mouth opening displacements. These differ significantly with test geometry; averaging 0.05 mm for four point bend tests and 0.09 mm for ring-on-ring tests. In uniaxial loading the crack opening displacement correlates with crack depth and the mode I stress intensity factor at the deepest points of the crack front [4]. Assuming similar characteristic crack depths in all tests, and that unstable fracture propagates from a point along the sub-surface crack front, the critical maximum mode I stress intensity factor at this position differs significantly with loading geometry. At the failure stress, this mode I stress intensity factor is lower for the equi-biaxial state, and cannot explain the relative strengths. This, and the larger opening displacements that are indicative of higher strains, imply that a critical strain energy release rate is the likely criteria to explain the difference in failure stress with loading geometry. Studies of crack opening compliance and more detailed FE modelling of the crack strain fields are in progress to investigate this further.

## SUMMARY

- Digital image correlation is a useful tool to detect and analyse crack nucleation and propagation in graphite under uniaxial and equi-biaxial flexural loading.
- The mean flexural strength of graphite under equi-biaxial loading is 17% lower than for uniaxial loading.
- It is suggested that a critical strain energy release rate controls fracture propagation under uniaxial and equi-biaxial stress states.

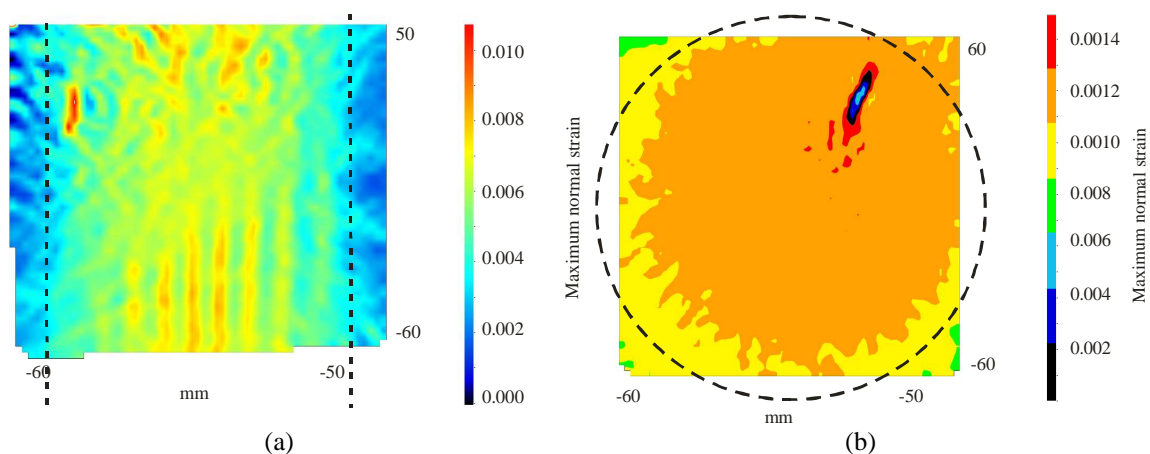


Figure 8- Maximum normal strain of an approximately  $100 \times 100 \text{ mm}^2$  window (a) uniaxial at  $\sigma_b = 27.46 \text{ MPa}$  (b) equi-biaxial at  $\sigma_b = 23.08 \text{ MPa}$

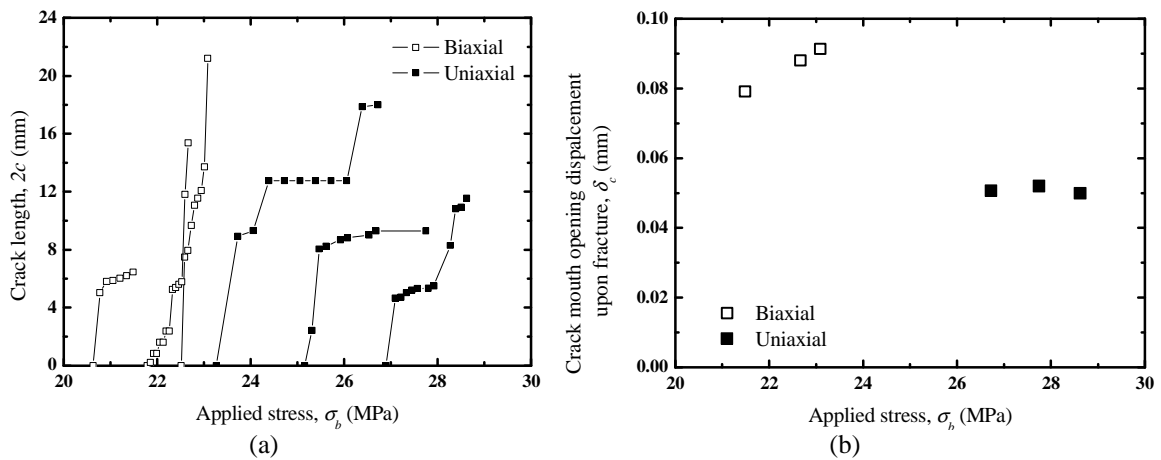


Figure 9- Crack characterisation of uniaxially and equi-biaxially loaded specimens  
(a) crack length (b) crack mouth opening displacement immediately prior to fracture

## ACKNOWLEDGEMENTS

The authors gratefully acknowledge the support of British Energy, part of EDF Energy, for this work under project GRA/GNSR/6041. The opinions expressed are those of the authors and not necessarily those of British Energy.

## REFERENCE

1. Tucker, M.O., in *IAEA Technical committee meeting on Mechanical behaviour of graphite for high temperature reactors*. 1979, IAEA: Gif sur Yvette, France.
2. Burchell, T.D., *Carbon*, 1996. **34**(3): p. 297-316.
3. Joyce, M.R., T.J. Marrow, T.J. Mummery, and B.J. Marsden, *Engineering Fracture Mechanics*, 2008. **75**(2): p. 3633-3645.
4. Li, H., J. Duff, and T.J. Marrow, in *PVP2008*. 2009, American Society of Mechanical Engineers: Chicago, Illinois
5. Morrell, R. 1998, NPL.
6. ABAQUS. 2008: ABAQUS Inc., Providence, Rhode Island, Version 6.9.
7. Hodgkin, A.D. 2006, The University of Manchester: Manchester.
8. Timoshenko, S. and S. Woinowsky-Krieger. 1959, New York: McGraw-Hill.
9. Li, F.Z., C.F. Shih, and A. Needleman, *Engineering Fracture Mechanics*, 1985. **21**(2): p. 405-421.
10. Newman, J.C. and I.S. Raju, *Engineering Fracture Mechanics*, 1981. **15**(1-2): p. 185-192.